JACS
JOURNAL OF THE AMERICAN CHEMICAL SOCIETY
Article
pubs.acs.org/JACS

Molecular Engineering of Organophosphate Hydrolysis Activity from a Weak Promiscuous Lactonase Template

Monika M. Meier,[†] Chitra Rajendran,[†] Christoph Malisi,[‡] Nicholas G. Fox,[§] Chengfu Xu,[§] Sandra Schlee,[†] David P. Barondeau,[§] Birte Höcker,[‡] Reinhard Sterner,[†] and Frank M. Raushel*[,§]

[†]Institute of Biophysics and Physical Biochemistry, University of Regensburg, Regensburg, Germany
[‡]Max Planck Institute for Developmental Biology, Tübingen, Germany
[§]Department of Chemistry, Texas A&M University, College Station, Texas 77842, United States

Supporting Information

ABSTRACT: Rapid evolution of enzymes provides unique molecular insights into the remarkable adaptability of proteins and helps to elucidate the relationship between amino acid sequence, structure, and function. We interrogated the evolution of the phosphotriesterase from *Pseudomonas diminuta* (*Pd*PTE), which hydrolyzes synthetic organophosphates with remarkable catalytic efficiency. PTE is thought to be an evolutionarily "young" enzyme, and it has been postulated that it has evolved from members of the phosphotriesterase-like lactonase (PLL) family that show promiscuous organophosphate-degrading activity. Starting from a weakly promiscuous PLL scaffold (*Dr*0930 from *Deinococcus radiodurans*), we designed an extremely efficient organophosphate hydrolase (OPH) with broad substrate specificity using rational and random mutagenesis in combination with in vitro activity screening. The OPH activity for seven organophosphate substrates was simultaneously enhanced by up to 5 orders of magnitude, achieving absolute values of catalytic efficiencies up to 10^6 M^{-1} s^{-1}. Structural and computational analyses identified the molecular basis for the enhanced OPH activity of the engineered PLL variants and demonstrated that OPH catalysis in *Pd*PTE and the engineered PLL differ significantly in the mode of substrate binding.

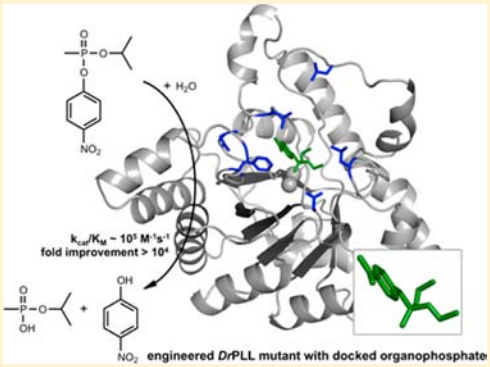

INTRODUCTION

Organophosphate nerve agents are among the most toxic compounds that have been chemically synthesized. These compounds are lethal because they rapidly inactivate acetyl cholinesterase, a key enzyme in the proper functioning of the nervous system.[1,2] Since the discovery of their biological activity, organophosphates have been widely used as broad-spectrum insecticides for agricultural and domestic applications[3] and have been exploited as chemical warfare agents for military use.[4] Organophosphate-hydrolyzing enzymes have been identified in Archaea, Bacteria, and Eukarya.[5] These metal-dependent organophosphate hydrolases (OPH) differ widely in three-dimensional structure and catalytic mechanism.[6] The phosphotriesterase (PTE) from *Pseudomonas diminuta* (*Pd*PTE) is the most active organophosphate-degrading enzyme that has been functionally and structurally characterized. The kinetic constants, k_{cat} and k_{cat}/K_M, for the hydrolysis of the insecticide paraoxon are 4.9×10^3 and 3.8×10^7 M^{-1} s^{-1}, respectively, with an overall rate enhancement of 10^{12}, relative to the uncatalyzed rate at pH 7.[7,8] The k_{cat}/K_M value for the *Pd*PTE-catalyzed hydrolysis of paraoxon approaches the diffusion-controlled limit for an encounter complex between enzyme and substrate.[9]

Phosphotriesterase-like lactonases (PLL) are the closest known structural homologues to *Pd*PTE, although the sequence identity is only ~30%. *Pd*PTE and related PLL enzymes share a similar $(\beta/\alpha)_8$-barrel structural fold and possess a binuclear metal center within the active site. Major structural differences are in the length and conformation of the $\beta\alpha$-loops (Supporting Information Figures S1 and S2). These enzymes belong to the amidohydrolase superfamily (AHS) of enzymes in cluster 1735 of orthologous groups (cog1735).[10] The primary catalytic activity of PLL enzymes is the hydrolysis of small molecular weight lactones, including homoserine lactone. These proteins also possess very weak promiscuous activity for the hydrolysis of organophosphates. The PLL from *Deinococcus radiodurans* (*Dr*PLL) has been structurally and functionally characterized.[11] *Dr*PLL is a robust, thermostable (T_M = 88 °C), and highly soluble protein, exhibiting weak promiscuous activity for the hydrolysis of methyl and ethyl paraoxon.[11,12] *Pd*PTE is thought to have evolved relatively recently to provide soil bacteria the ability to utilize organophosphate compounds as energy and nutrient sources.[13,14] The reactions catalyzed by PLL and *Pd*PTE enzymes

Received: June 12, 2013
Published: July 9, 2013

dx.doi.org/10.1021/ja405911h | J. Am. Chem. Soc. 2013, 135, 11670−11677

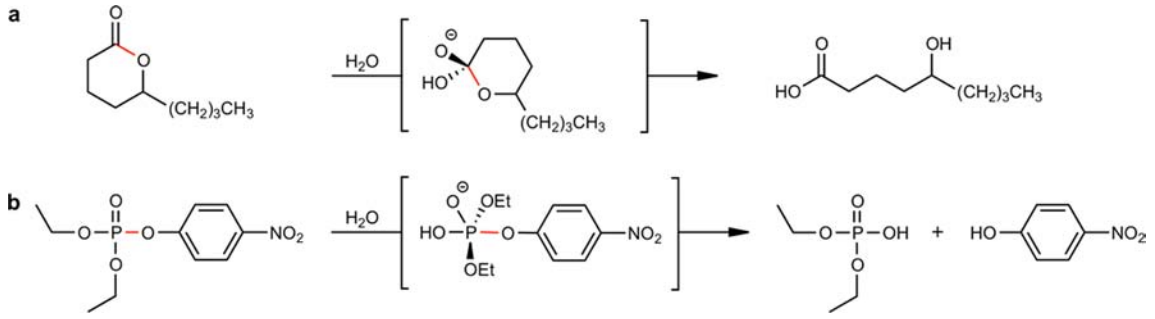

Figure 1. Reaction schemes for the hydrolysis of lactones and organophosphate triesters. (a) Hydrolysis of δ-nonanoic lactone to 5-hydroxy nonanoic acid via a tetrahedral transition state. (b) Hydrolysis of paraoxon to diethyl phosphate via a trigonal bipyramidal transition state.

involve the nucleophilic attack of water (or hydroxide), but the transition-state geometries for the two reactions are distinct (Figure 1). PLL enzymes exhibit promiscuous organophosphatase activity, which may be due to the physical similarities between the reactive intermediate for the native lactonase reaction and the ground/intermediate state for the PTE reaction.[15]

Here, we report the generation of an efficient and broad-spectrum organophosphate hydrolase starting from the *Dr*PLL scaffold with a weakly promiscuous organophosphate-hydrolyzing activity. Using rational and random mutagenesis approaches, in combination with in vitro screening, we have enhanced the PTE activity for seven different organophosphate substrates by up to 5 orders of magnitude, achieving absolute values of catalytic activity of 10^6 M^{-1} s^{-1}. These values approach the rate constants for many natural enzymes.[16] Structural and computational analyses identified the structural basis for the enhanced PTE activity of the engineered *Dr*PLL variants, thus providing mechanistic insights into the evolutionary pathway from PLL to PTE.

MATERIALS AND METHODS

Materials. Organophosphate compounds (**OP 1**−**8**, diisopropyl methyl phosphonate and diethyl 4-methylbenzylphosphonate) were supplied by Sigma-Aldrich, Alfa Aesar, or synthesized by modifications of published procedures.[17−19]

Protein Expression and Purification. Genes encoding *Pd*PTE variants and *Dr*PLL variants were subcloned into pET plasmids and expressed in *Escherichia coli* BL21(DE3) and *E. coli* BL21(DE3) Rosetta 2 cells (Merck), respectively. The recombinant proteins were purified from the soluble cell extract by anion exchange chromatography (and size exclusion chromatography) after an initial protamine sulfate and ammonium sulfate purification step. Protein purity and integrity was verified by SDS-PAGE. Protein concentrations were determined spectrophotometrically using the calculated molar extinction coefficient of 29910 M^{-1} cm^{-1} for wild-type *Dr*PLL and 29 450 M^{-1} cm^{-1} for wild-type *Pd*PTE. Further details of the methods used are described in Supporting Information.

Enzyme Kinetics. The organophosphatase activity and δ-nonanoic lactone hydrolytic activity of purified *Dr*PLL variants and wild-type *Pd*PTE were determined at 30 °C using colorimetric assays. The PTE activity for *p*-nitrophenol-substituted compounds was monitored by following the release of *p*-nitrophenol at 400 nm (ε_{400} = 17 000 M^{-1} cm^{-1}). Reactions were performed in 50 mM CHES, pH 9.0, 100 μM $CoCl_2$, and various concentrations of substrate. For compounds **OP 4** and **OP 5**, the reaction assay was supplemented with 12% MeOH. Hydrolysis reactions with **OP 8** were performed in 50 mM HEPES, pH 8.0, 0.3 mM DTNB, 100 μM $CoCl_2$, 12% MeOH, and variable concentrations of **OP 8** (0−3.5 mM). The reaction was monitored at 412 nm (ε_{412} = 1.42 × 10^4 M^{-1} cm^{-1}). The hydrolysis of δ-nonanoic lactone was monitored using a pH-sensitive colorimetric assay.[20] The reactions were performed in 2.5 mM BICINE, pH 8.3, 0.1 mM $CoCl_2$, 1.4% DMSO, 0.1 mM *m*-cresol purple, 0.2 M NaCl, and various concentrations of substrate (0−2 mM). The change in absorbance at 577 nm was monitored. Initial rates were determined and fit to the Michaelis−Menten equation $v/E_t = (k_{cat}[S])/(K_M + [S])$ to obtain values of k_{cat} and K_M. If applicable, the enzyme was diluted in buffer supplemented with 1 mg/mL bovine serum albumin. Bovine serum albumin has no influence on OPH activity.

Library Construction and Screening. The plasmid-encoded error-prone library was generated on the *Dr*PLL wild-type template as previously described.[21] The pTNA-*drpll* library contained 2.7 × 10^7 independent variants and resulted in approximately six nucleotide exchanges per gene. For generating libraries of shuffled genes, selected *Dr*PLL variants were applied to the staggered extension process.[22] The assembly PCR reaction was further amplified by nested PCR, digested with *Sph*I and *Hin*dIII (New England Biolabs), and recloned into pTNA vector for low constitutive expression. The targeted libraries were constructed using synthetic oligonucleotides and overlap extension PCR[23] or QuikChange Mutagenesis.[24] Further details of the methods used are described in Supporting Information.

Randomly picked colonies from *E. coli* BL21-CodonPlus(DE3) cells transformed with the libraries were individually grown in 96-well plates overnight, in Super Broth media supplemented with 1 mM $CoCl_2$. Cells were lysed by incubation 1× BugBuster (Merck) in 50 mM HEPES, pH 8.5, 100 μM $CoCl_2$, and incubated for 30 min at room temperature. The crude lysate was used to assay the PTE activity using the racemic compounds in 50 mM CHES, pH 9.0, and *p*-nitrophenol release was measured at 400 nm using an absorbance plate reader.

X-ray Structure Determination and Docking. Crystallization of *Dr*PLL.8, *Dr*PLL.9, and *Dr*PLL.10 variants is described in Supporting Information. The X-ray structures of *Dr*PLL variants were solved by molecular replacement, using the published wild-type *Dr*PLL structure (PDB ID: 3FDK) as template. Data collection and refinement statistics are shown in Table S5. **OP 7** was docked into the active site of the *Dr*PLL.10 structure using the RosettaLigand program.[25,26] Further details of the methods used are described in Supporting Information.

Determination of Stereoselectivity. The stereoselectivity of the *Dr*PLL variants when reacting with chiral organophosphates was determined with racemic compounds as substrates using the previously reported stereoselectivity of wild-type *Pd*PTE and two engineered *Pd*PTE mutants (*Pd*PTE-G60A and *Pd*PTE-H254G+H257W+L303T) for 4-acetylphenol leaving group analogues of **OP 1**−**5**.[17] Approximately 50 μM organophosphate substrate was incubated with various amounts of enzyme in 50 mM CHES, pH 9.0, 100 μM $CoCl_2$ at 30 °C, and the release of *p*-nitrophenol was monitored as a function of time by measuring the absorbance at 400 nm. To identify the configuration of the nonhydrolyzed isomer in solution after the reaction approached an end point at approximately half amplitude, wild-type *Pd*PTE or engineered *Pd*PTE variants were added to the reaction mixture, inducing the (exclusive) hydrolysis of the residual S_P enantiomer. The change of absorbance over time was exponential. Depending on the compound and enzyme variant used, one or two phases were observed and fit to a single exponential $(A(t) = y_0 + a(1 - e^{-k1t}))$ or double exponential fit $(A(t) = y_0 + a(1 - e^{-k1t}) + b(1 - e^{-k2t}))$. As the

dx.doi.org/10.1021/ja405911h | J. Am. Chem. Soc. 2013, 135, 11670−11677

substrate concentration was kept below the K_M value, the time course follows pseudo-first-order kinetics, and the associated rate constants are directly proportional to the amount of enzyme added.[27,28] The catalytic efficiency, k_{cat}/K_M, was estimated from the exponential components according to $k_{cat}/K_M = k_x/[E]$.

RESULTS

_Dr_PLL and _Pd_PTE Are Mutually Promiscuous. Wild-type *Dr*PLL and *Pd*PTE were analyzed for their ability to hydrolyze lactones and organophosphates. Catalytic activity of *Dr*PLL was assayed with a broad set of organophosphates (**OP 1−7**; Chart 1), and low promiscuous activity was found for the hydrolysis of methylphosphonates (**OP 1−5**) and phosphotriesters (**OP 6−7**). The values of k_{cat}/K_m are 4−7 orders of magnitude lower when compared with the k_{cat}/K_m values of *Pd*PTE with the same set of compounds (Table 1). Conversely, the lactonase activity of wild-type *Pd*PTE for the hydrolysis of δ-nonanoic lactone (k_{cat}/K_m = 68 M^{-1} s^{-1}) is 5 orders of magnitude lower than the catalytic efficiency of *Dr*PLL with this substrate ($k_{cat}/K_m = 7.9 \times 10^6$ M^{-1} s^{-1}) (Table S1). With regards to their respective promiscuous substrates, both enzymes exhibit very low k_{cat}/K_m values. Since wild-type *Dr*PLL exhibits measurable, but weak, activity for a broad spectrum of organophosphates, this protein scaffold was selected as a suitable starting point for the evolution of an effective organophosphate degrading enzyme.

Chart 1. Structures of Compounds Tested as Substrates for Evolved *Dr*PLL

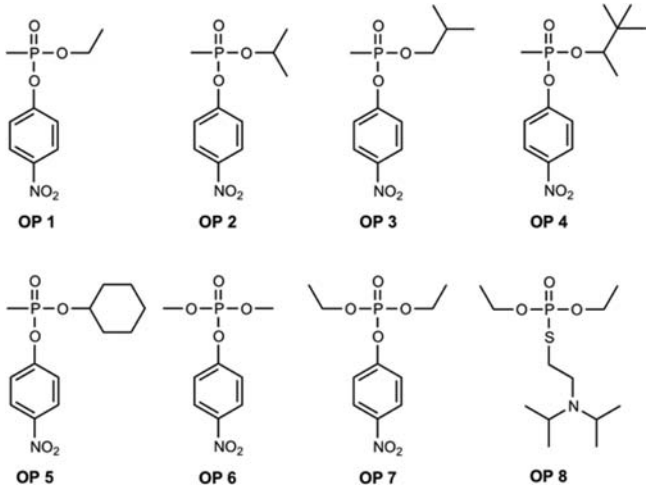

Evolution of _Dr_PLL for Broad-Spectrum Organophosphate Hydrolysis. To obtain insight into the structural requirements for the acquisition of enhanced organophosphatase activity from wild-type *Dr*PLL, an interative mutagenic protocol was devised. In this strategy, rational protein design and random mutagenesis methodologies were combined with an efficient in vitro screening to identify highly efficient hydrolase variants with enhanced degradation capacity toward **OP 1−7** (Chart 1). An overview of mutagenic methods and identified mutations is given in Figure 2. Initially, random mutations were introduced into wild-type *Dr*PLL using error-prone PCR, and the protein library was subsequently screened for catalytic activity with paraoxon (**OP 7**). Improved catalytic activity was identified with mutations at several residue positions including Tyr-28, Asp-71, Glu-179, Val-235, Leu-270, and Pro-274 (Figure 2). The most proficient variant isolated at this stage, *Dr*PLL.1 (D71N/E179D/L270M), exhibited a 25-fold increase in catalytic efficiency (k_{cat}/K_m of 7.2×10^2 M^{-1} s^{-1}) relative to wild-type *Dr*PLL for the hydrolysis of paraoxon. Although the library was not screened for catalytic activity toward methyl paraoxon (**OP 6**) and the five methyl phosphonates (**OP 1−5**), the epPCR variant showed increased catalytic activity with most of these compounds. The highest catalytic efficiency was obtained with **OP 2** (1.4×10^3 M^{-1} s^{-1}), displaying an increase in catalytic activity of more than 2 orders of magnitude, relative to wild-type *Dr*PLL. The kinetic constants for the hydrolysis of **OP 1** through **OP 7** by *Dr*PLL.1 are presented in Tables 1 and 2.

The genes encoding the four best variants, *Dr*PLL.1, *Dr*PLL.2 (A3T/G38R/T105S/P274L), *Dr*PLL.3 (V35E/A103V), and *Dr*PLL.4 (R272C) for the hydrolysis of paraoxon were recombined in vitro with wild-type *Dr*PLL and another variant (F26G/C72I)[11] using the staggered extension process (StEP).[22] The library was screened for hydrolytic activity with paraoxon, and a beneficial glycine residue was identified in place of Glu-101. However, substantial increases in the hydrolysis of paraoxon were not obtained for the variants isolated from the StEP approach. The mutations E101G and V235L have previously been described by Hawwa et al. as organophosphate-degrading activity-enhancing mutations.[12] The fact that these residue positions have now been identified in two independent screens emphasizes the importance of these particular sites. The two beneficial exchanges (V235L and E101G) were subsequently combined with mutations in the *Dr*PLL.1 template yielding the variant *Dr*PLL.7 (D71N/E101G/E179D/V235L/L270M) (Figure 2). The catalytic efficiencies for the hydrolysis of methyl paraoxon and paraoxon improved 4−5-fold, while the catalytic parameters for **OP 1−5** remained essentially unchanged (Tables 1 and 2).

Since our aim was to achieve a simultaneous increase in the catalytic efficiencies toward all organophosphate substrates, smaller and more focused libraries were generated and screened with **OP 1−7** simultaneously, while concurrently reducing the substrate concentrations gradually to obtain improvements in

Table 1. Catalytic Efficiencies (k_{cat}/K_M [M^{-1} s^{-1}]) for *Dr*PLL, Selected Mutants, and *Pd*PTE at pH 9.0

OP	*Dr*PLL	*Dr*PLL.1	*Dr*PLL.7	*Dr*PLL.8	*Dr*PLL.9	*Dr*PLL.10	*Pd*PTE
1	6.1×10^2	5.0×10^2	6.7×10^2	7.9×10^3	2.2×10^4	2.5×10^5	1.3×10^7
2	9.8×10^0	1.4×10^3	1.1×10^3	6.2×10^3	4.3×10^4	3.6×10^5	1.0×10^7
3	5.1×10^0	1.0×10^3	1.2×10^3	6.2×10^3	4.0×10^4	3.5×10^5	8.5×10^6
4	6.8×10^0	3.7×10^2	2.4×10^2	8.1×10^2	3.5×10^3	9.2×10^3	1.2×10^4
5	2.1×10^0	4.4×10^2	2.4×10^2	1.2×10^3	6.0×10^3	3.5×10^4	6.6×10^5
6	2.0×10^2	6.6×10^1	2.8×10^2	1.6×10^3	8.0×10^3	3.4×10^4	2.4×10^7
7	2.9×10^1	7.2×10^2	3.6×10^3	7.6×10^3	1.6×10^4	2.0×10^4	1.2×10^8

dx.doi.org/10.1021/ja405911h | J. Am. Chem. Soc. 2013, 135, 11670−11677

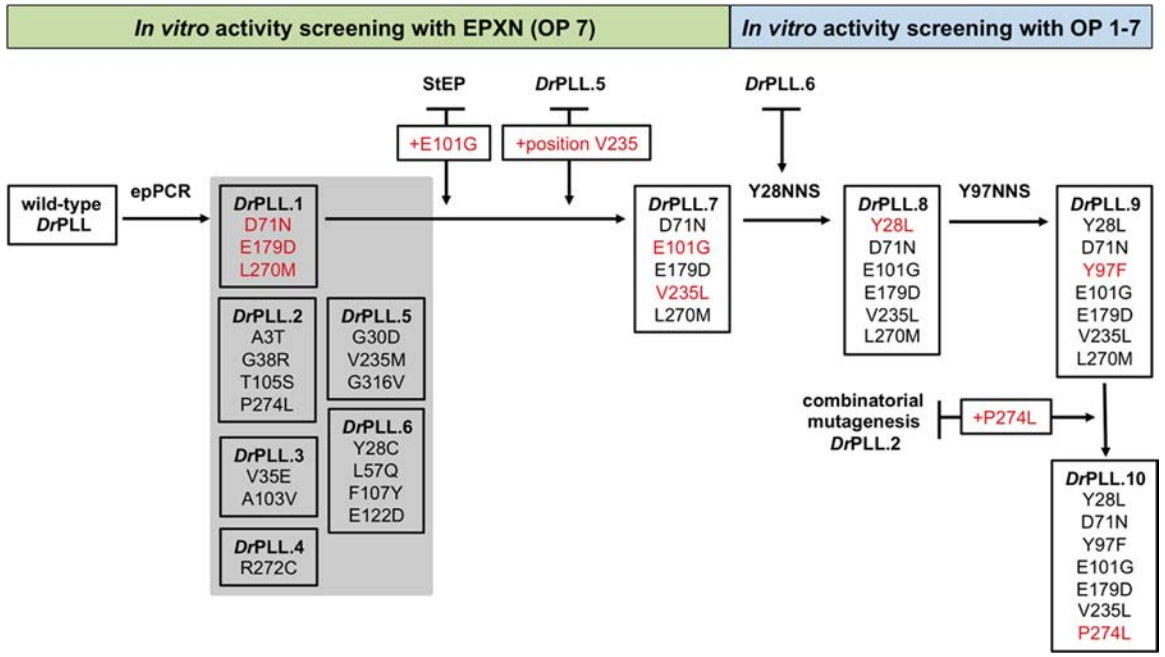

Figure 2. Overview of the experimental strategy. The boxes illustrate the engineered *Dr*PLL variants. Amino acid exchanges in red are mutations that were newly identified in the individual steps. The applied mutagenesis technique is stated above the arrow. EpPCR yielded 12 beneficial variants, the six most important are shown. These variants contain an additional T2Q exchange, which is thought to have no effect on OPH activity. *Dr*PLL.1−*Dr*PLL.4, *Dr*PLL-F26G-C72I,[11] and wild-type *Dr*PLL were recombined by StEP. The StEP technique identified the mutation E101G. Positions Y28 and F97 were randomized by site-saturation mutagenesis. Bona fide beneficial exchanges of variants *Dr*PLL.2 and *Dr*PLL.4 were added in various combinations to template *Dr*PLL.9. The best variant was *Dr*PLL.10.

Table 2. Turnover Numbers (k_{cat} [s^{-1}]) for *Dr*PLL, Selected Mutants, and *Pd*PTE at pH 9.0

OP	*Dr*PLL	*Dr*PLL.1	*Dr*PLL.7	*Dr*PLL.8	*Dr*PLL.9	*Dr*PLL.10	*Pd*PTE
1	3.0×10^{-1}			3.1×10^{0}			9.6×10^{3}
2		2.4×10^{0}	3.6×10^{0}	3.1×10^{0}	2.2×10^{1}	6.8×10^{1}	4.3×10^{3}
3	2.6×10^{-2}	3.6×10^{0}	3.0×10^{0}	2.6×10^{0}	1.9×10^{1}	1.3×10^{2}	3.4×10^{3}
4	1.2×10^{-2}	2.1×10^{0}		1.2×10^{0}	7.5×10^{0}	9.4×10^{0}	8.8×10^{1}
5				1.4×10^{0}	1.3×10^{1}	4.0×10^{1}	1.5×10^{3}
6	5.0×10^{-2}	7.5×10^{-1}	4.4×10^{0}	2.3×10^{0}	8.0×10^{0}	4.2×10^{1}	2.6×10^{4}
7	5.7×10^{-2}	4.7×10^{0}	5.4×10^{0}	2.9×10^{0}	1.3×10^{1}	1.1×10^{1}	1.7×10^{4}

k_{cat}/K_m.[29] Successive saturation mutagenesis at residue positions Tyr-28 (identified in *Dr*PLL.6) and Tyr-97 led to the identification of variants *Dr*PLL.8 (*Dr*PLL.7 + Y28L) and *Dr*PLL.9 (*Dr*PLL.8 + Y97F). In all of these mutants, the kinetic constants improved significantly for **OP 1−7** (Tables 1 and 2). The most active mutant, *Dr*PLL.9, reached a catalytic efficiency of 4.3×10^4 M^{-1} s^{-1} for the hydrolysis of **OP 2**. The highest fold improvements, relative to wild-type *Dr*PLL, were obtained with **OP 2** (4.4×10^3) and **OP 3** (7.8×10^3). Combinatorial mutagenesis was subsequently conducted with other mutational sites (G38R, T105S, P274L, and R272C) that were identified in earlier epPCR experiments (variants *Dr*PLL.2 and *Dr*PLL.4). A total of 15 combinatorial mutants were constructed and screened for the hydrolysis of **OP 1−7**. These experiments resulted in the identification of *Dr*PLL.10 (DrPLL.9 − L270 M + P274L; Figure 2). This mutant contains seven amino acid exchanges, relative to the wild-type enzyme, and is able to catalyze the hydrolysis of selected organophosphates up to 5 orders of magnitude faster relative to wild-type *Dr*PLL (Figure 3). The best substrate (**OP 2**) is hydrolyzed with a k_{cat}/K_M of 3.6×10^5 M^{-1} s^{-1} (Table 1).

Native Activity and Stereoselectivity. The engineered *Dr*PLL variants were characterized for their residual native lactonase activities and stereoselective hydrolysis of chiral organophosphate substrates. While organophosphatase activity increased substantially, there was a trade-off for the hydrolysis of the native δ-nonanoic lactone substrate (Table S1). *Dr*PLL.10 has a value of k_{cat}/K_M for the hydrolysis of δ-nonanoic lactone of 2.8×10^3 M^{-1} s^{-1}, which corresponds to a decrease in catalytic activity of 2800-fold, while the catalytic efficiencies for the hydrolysis of organophosphates increased up to 6.9×10^4-fold (Table 1).

The *Dr*PLL mutants were initially screened with racemic mixtures of chiral organophosphates (**OP 1−5**) that are chromophoric analogues of the nerve agents VX, GB, VR, GD, and GF, respectively. To assess the stereoselectivity of these enzymes, the enantiomeric preferences of wild-type *Dr*PLL and *Dr*PLL.10 were determined with the methylphosphonate substrates by measuring the complete time courses for the hydrolysis of the racemic compounds at high and low enzyme concentrations (Figure S3). Wild-type *Dr*PLL and *Dr*PLL.10 preferentially hydrolyze the less toxic R_P enantiomers of **OP 1−5** (Table S2). This equals the stereoselectivity of wild-type *Pd*PTE.[17] Remarkably, evolution of faster hydrolysis rates for the chromophoric analogues of the G- and V-type nerve agents was accompanied by an

dx.doi.org/10.1021/ja405911h | J. Am. Chem. Soc. 2013, 135, 11670−11677

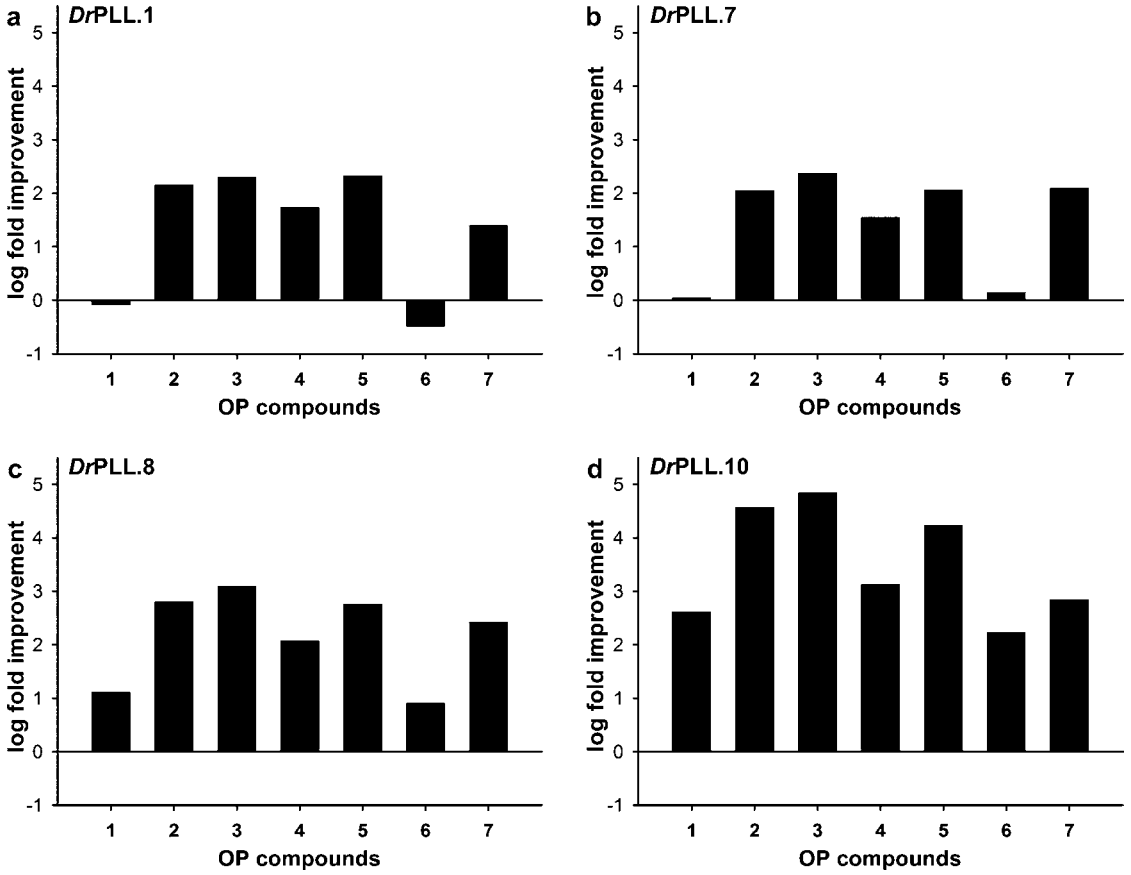

Figure 3. Comparison of the catalytic parameters of *Dr*PLL.1, *Dr*PLL.7, *Dr*PLL.8, and *Dr*PLL.10 with those of wild-type *Dr*PLL. The improvements of the four mutant enzymes in the values of k_{cat}/K_M relative to those of wild-type *Dr*PLL for compounds **OP 1** through **OP 7** (from the values in Table 1) are presented.

enhancement in the overall stereoselectivity except for **OP 1** (Table S3). The highest enantiomeric preference was observed with **OP 2**. The highest values of k_{cat}/K_m (1.1×10^6 M^{-1} s^{-1}) for any substrate were obtained with the R_P enantiomers of **OP 1** and **OP 3** (Table S2).

Wild-type *Dr*PLL and selected mutant enzymes were tested for their ability to hydrolyze P−S bonds using a phosphothioester analogue of the nerve agent VX (**OP 8**). However, the rate constants for the hydrolysis for this compound by the various mutants were very low (k_{cat}/K_m = ~1 M^{-1} s^{-1}), and there was no significant improvement in the rate of hydrolysis with respect to wild-type *Dr*PLL (Table S4).

Crystal Structures of Selected *Dr*PLL Mutants. The crystal structures of *Dr*PLL.8 (PDB ID: 4J5N), *Dr*PLL.9 (PDB ID: 4J2M), and *Dr*PLL.10 (PDB ID: 4J35) were determined to resolutions of 1.78−2.05 Å (Table S5). A structural superposition of wild-type *Dr*PLL and *Dr*PLL.10 is presented in Figure 4a. The two metal binding sites and the metal-coordinating residues (His-21, His-23, carboxylated Lys-143, His-176, His-204, and Asp264) were retained in the mutated proteins. The side chain of the active site residue Arg-228 adopts an alternate conformation relative to wild-type *Dr*PLL (Figure 4b). Except for Trp-269 ($\beta\alpha$-loop 8) and Met-234 ($\beta\alpha$-loop 7), all invariable residues in the substrate binding pocket of *Dr*PLL.10 align well with the residues in wild-type *Dr*PLL. The structural changes around the mutated positions are illustrated in Figure S4 for *Dr*PLL.10. The $\beta\alpha$-loop 1 contains the mutation Y28L. The introduction of the smaller, hydrophobic amino acid increases the size of the active site, providing more space for the accommodation of the larger organophosphate substrates. The $\beta\alpha$-loop 3, composed of residues Phe-96 to Glu-117, was displaced by up to 3 Å at residue positions Ala-99 to Ala-103, due to the elimination of a hydrogen bond between the side chain of Asp-71 ($\beta\alpha$-loop 2) and the backbone nitrogen of Ala-103. The E101G mutation, like Y28L, enlarges the substrate binding pocket. The side chain of Phe-97, present in *Dr*PLL.9 and *Dr*PLL.10, overlaps in the case of *Dr*PLL.10 the side chain of Tyr-97 in the wild-type enzyme.

The E179D mutation in $\beta\alpha$-loop 5 adopts an alternate conformation within the engineered variants. In *Dr*PLL.10, residue Asp-179 does not form a hydrogen bond to the neighboring Arg-148 in $\beta\alpha$-loop 4, resulting in more flexibility. The $\beta\alpha$-loop 7 is composed of residues Arg-228 to Thr-239. This loop is in a similar conformation as an alternate *Dr*PLL wild-type structure (PDB ID: 2ZC1), providing no obvious explanation for the considerable increase in activity caused by the V235L mutation. The mutation L270 M ($\beta\alpha$-loop 8), present in *Dr*PLL.8 and *Dr*PLL.9, is found in a location remote from the active site. The P274L mutation, present only in *Dr*PLL.10, causes a shift of the backbone by 1.7 Å (Figure S4b).

Computational Docking. Attempts to obtain complexed structures of the *Dr*PLL variants by cocrystallization with substrate and product analogues or soaking of preformed crystals failed. Therefore, the substrate **OP 7** was computationally docked using the RosettaLigand program[25] into the active site of *Dr*PLL.10 to assess the conformational and spatial orientation of the bound substrate. This docking program has

dx.doi.org/10.1021/ja405911h | J. Am. Chem. Soc. 2013, 135, 11670−11677

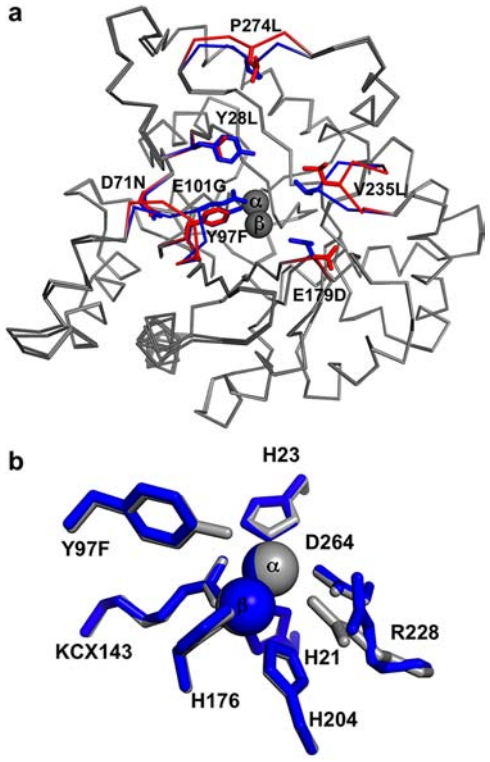

Figure 4. Structural superposition of *Dr*PLL.10 (PDB ID: 4J35) and *Dr*PLL (PDB ID: 3FDK). (a) Cα atoms of *Dr*PLL.10 and wild-type *Dr*PLL superimpose with an rmsd of 0.42 Å. The seven mutations are indicated (blue sticks, wild-type *Dr*PLL residues; red sticks, *Dr*PLL.10 residues). The largest backbone differences are observed in $\beta\alpha$-loops 3 (mutations Y97F and E101G) and 8 (mutation P274L). Some variation can also be seen in $\beta\alpha$-loop 7 (mutation V235L). (b) Active site superposition of wild-type *Dr*PLL (depicted in gray) and *Dr*PLL.10 (depicted in blue). The metal-coordinating histidine and aspartate residues maintain their wild-type conformation. The active site residue R228 adopts an alternate conformation.

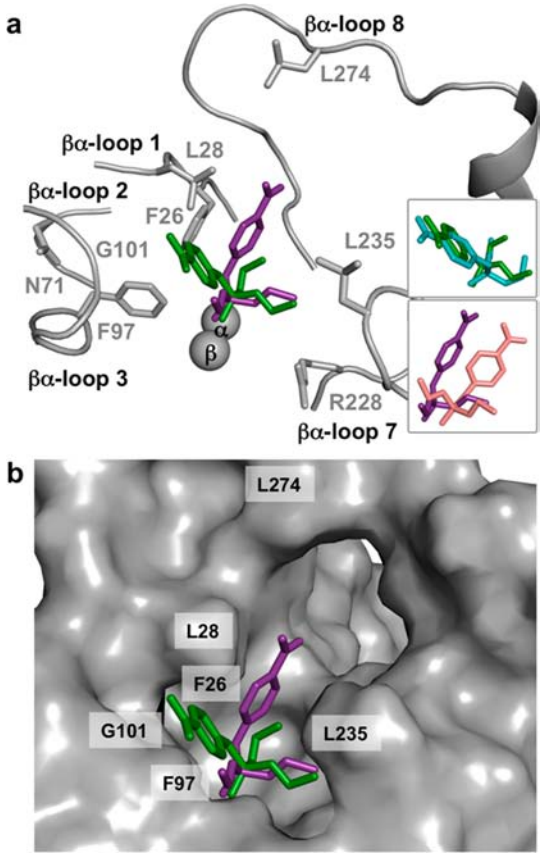

Figure 5. Docking poses of paraoxon (**OP 7**) in the crystal structure of *Dr*PLL.10, obtained with the RosettaLigand program using distance and angle constraints. (a) Active site and substrate binding pocket of *Dr*PLL.10. One representative of each cluster of docking poses of **OP 7** is shown in green and purple, respectively. The docking pose depicted in green belongs to the group of highest-scoring and most frequently occupied cluster of docking poses; the docking pose in purple belongs to the second cluster of docking poses. The variation within each cluster of docking poses is indicated in the insets. Docking poses for the first cluster are illustrated in green and cyan; the second cluster of docking poses is depicted in purple and light pink. Residue side chains of Arg-228 and Leu-274 adopt a different conformation in the docked structure compared to the conformation obtained by crystallization. The Arg-228 side chain is shifted in order to accommodate the ligand (only one Arg-228 side chain conformation is shown). (b) Active site and substrate binding pocket of *Dr*PLL.10 in surface representation.

been successfully applied in the docking of organophosphates and lactones in adenosine deaminase and paraoxonase 1 (PON1).[26,30] Initially, retrospective docking with wild-type *Pd*PTE using diisopropyl methyl phosphonate (DIMP) and **OP 7** was performed, yielding docking poses that were essentially identical to poses observed by crystallization (Figure S5).[31] **OP 7** was subsequently docked into the active site of *Dr*PLL.10. When no external constraints were set, the phosphoryl oxygen of **OP 7** hydrogen bonded to the side chain of Arg-228, indicating a potential electrostatic interaction of the guanidine group to the substrate (Figure S6). Since the inhibitor complexes of PTE always show an electrostatic interaction between M_β and the phosphoryl oxygen of the inhibitor, molecular constraints as derived from DIMP-complexed *Pd*PTE structure (PDB ID: 1EZ2) were subsequently set to enforce a metal-complexed interaction. The phosphoryl oxygen of the ligand was restricted to reside within 2.5 ± 0.4 Å to M_β, and the angle between M_β and the phosphoryl oxygen (O═P) was set to 140 ± 30°.

The 20 top-scoring docking poses were analyzed and yielded two clusters of poses (Figure 5). In the highest-scoring and most frequently occupied pose, the *p*-nitrophenyl ring is oriented toward $\beta\alpha$-loop 3. This is equivalent to the leaving group subsite in *Pd*PTE.[31,32] The two *O*-ethyl substituents fit within the large pocket generated by $\beta\alpha$-loops 7 and 8 in *Dr*PLL.10. In the second pose, the *p*-nitrophenyl moiety and one *O*-ethyl substituent fit within the large pocket; the second *O*-ethyl substituent is oriented toward $\beta\alpha$-loop 3. The orientation of representative docking poses for paraoxon in the substrate binding pocket of *Dr*PLL.10 are shown in Figure 5. To compare the conformational and spatial orientation of paraoxon in *Dr*PLL.10 and *Pd*PTE, one of the best top-scoring paraoxon-docking poses for *Dr*PLL.10 was superimposed with the paraoxon-docking pose for *Pd*PTE (Figure S7). Docking of paraoxon yielded similar binding modes in *Dr*PLL.10 and *Pd*PTE with respect to the orientation of the *p*-nitrophenyl ring. However, the orientation of the *O*-ethyl substituents differs. The *O*-ethyl substituents cannot be accommodated in the same orientation as in *Pd*PTE due to a steric clash of one *O*-ethyl substituent with Phe-26 ($\beta\alpha$-loop 1); therefore, Phe-26 appears to be important for substrate positioning. Site-

dx.doi.org/10.1021/ja405911h | J. Am. Chem. Soc. 2013, 135, 11670−11677

saturation experiments confirmed a strong deleterious effect on organophosphatase activity when Phe-26 is substituted by any other residue. The equivalent residue in *Pd*PTE (G60) is crucial for *Pd*PTE activity.[32]

DISCUSSION

The results presented here dramatically demonstrate that controlled laboratory evolution can establish high organophosphatase activity on the *Dr*PLL scaffold. Together with a recent reverse functional transition experiment, where homoserine lactonase activity was established within the *Pd*PTE scaffold,[33] our results provide the first strong evidence for the evolution of PTE activity from members of the PLL family (Figure 6). A total of only three mutations was sufficient to substantially alter the substrate specificity of *Dr*PLL (*Dr*PLL.1 (D71N/E179D/L270M)). An extremely efficient PTE was created starting from a protein scaffold with barely detectable ability to hydrolyze organophosphates.

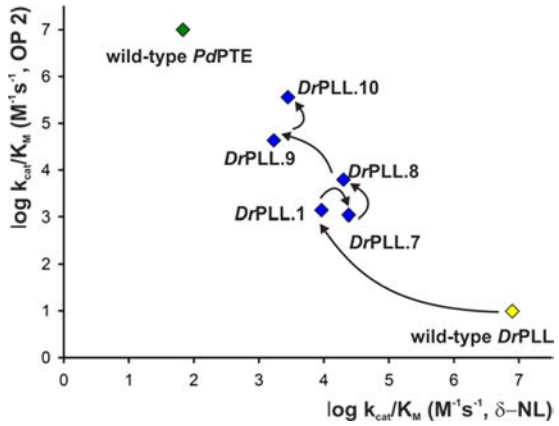

Figure 6. Relationship between lactonase and organophosphatase activity in the engineered mutants of *Dr*PLL and wild-type *Pd*PTE with the substrate **OP 2**.

In the reverse functional transition experiment, the mutation of H254R in PTE proved to be the key for the switch in activity from a phosphotriesterase to a lactonase[33]/esterase.[34] In our reconstruction of the active site of *Dr*PLL, Arg-228 is essential for the acquisition of organophosphatase activity. Mutation of this arginine residue to another polar amino acid, including histidine, leads to a dramatic loss in organophosphatase activity. Overall, our reconstruction of the active site within *Dr*PLL did not yield variants that simply rebuilt the *Pd*PTE active site structure evolved by natural evolution.

The overall increase in catalytic activity for the variants constructed for this investigation is attributed to a slight decrease in the K_M value for organophosphate substrates coupled with a substantial increase in k_{cat}. The catalytic efficiency for the hydrolysis of organophosphates by *Dr*PLL variants has been improved up to 6.9×10^4-fold. The k_{cat}/K_M values for the hydrolysis of methyl phosphonates **OP 1** to **OP 3** are particularly high and achieve absolute values of up to 3.6×10^5 M^{-1} s^{-1}. The catalytic efficiencies with the bulkier substituents (**OP 4** and **OP 5**), and the phosphotriesters (**OP 6** and **OP 7**) are lower by approximately 1 order of magnitude. *Dr*PLL.10 exhibits a value of k_{cat}/K_M of 10^4 M^{-1} s^{-1} for the hydrolysis of **OP 4**, which is identical to the catalytic efficiency of wild-type *Pd*PTE for this substrate ($k_{cat}/K_M \sim 10^4$ M^{-1} s^{-1}). Therefore, the results presented here underline the catalytic versatility of the ubiquitous $(\beta\alpha)_8$-barrel structural fold.[35] While work on these and related systems has been performed,[12,15,36−38] no comparable improvements in catalytic efficiencies for seven substrates simultaneously within a single structural template have been described.

Recently, Zhang et al. utilized site-saturation mutagenesis and whole-gene error-prone PCR approaches to enhance the phosphotriesterase activity of a thermostable lactonase from *Geobacillus kaustophilus* HTA426 (GkaP).[39] The wild-type GkaP enzyme (gil56420041) is 60% identical in amino acid sequence to *Dr*PLL. The best mutant of GkaP (F28I/Y99L/T171S/F228L/N269S/V270G/W271C/G273D) increased the value of k_{cat}/K_m for the hydrolysis of paraoxon (**OP 7**) by a factor of 230. Of the beneficial residue positions identified in GkaP, only Tyr-99 directly overlaps with the set of mutations identified in the best variant identified in this study, DrPLL.10 (see Figure S1). In *Dr*PLL.10, Tyr-97 was changed to a phenylalanine, and in the GkaP mutant, the equivalent residue (Tyr-99) was changed to a leucine.

Despite the trade-off in wild-type lactonase activity, the engineered *Dr*PLL.10 mutant is a truly bifunctional enzyme, exhibiting broad substrate specificity for the hydrolysis of lactones and organophosphate substrates (Figure 6). Protein designs with both weak and strong trade-offs between engineered promiscuous and original catalytic activities have been reported.[21,33,34,40−42] However, the conservation of the native lactonase function was not a constraint of the screen, which only searched for improved organophosphatase activity. Most likely, the structural flexibility of the $\beta\alpha$-loops and the conservation of most residues important for positioning of the native substrate (Arg-228, Asp-264, Phe-26, Leu-231, Val-235, and Trp-287) allowed for the retention of the native lactonase function. However, the deletion of a crucial electrostatic interaction in the mutation of Tyr-97 to phenylalanine and an overall enlargement of the active site led to reduced catalytic efficiencies for the hydrolysis of lactones relative to the wild-type enzyme. In wild-type *Dr*PLL, Tyr-97 coordinates M_β and this charge transfer interaction gives the protein a purple color. Overall, our results demonstrate quite clearly that the creation of an evolved active site within a lactonase template can be conducted with high efficiency and a relatively small number of amino acid changes. Altogether, the concerted efforts of directed evolution, structural biology, and computational docking enabled the design of a tailored and highly efficient enzyme.

ASSOCIATED CONTENT

Supporting Information

Steady-state kinetic parameters for hydrolysis of δ-nonanoic lactone and **OP 8**, stereoselectivity data, data collection and refinement statistics for mutant structures, structure and sequence-based comparative analysis of *Pd*PTE and *Dr*PLL, structural analysis of mutant structures, computational docking data, additional procedural details. This material is available free of charge via the Internet at http://pubs.acs.org.

AUTHOR INFORMATION

Corresponding Author

raushel@tamu.edu

Notes

The authors declare no competing financial interest.

■ ACKNOWLEDGMENTS

We thank Andrew Bigley for providing the DEVX substrate, *Pd*PTE variants, and kinetic parameters of wild-type *Pd*PTE for DEVX hydrolysis. We thank Jörg Claren and Rainer Merkl for discussion and comments on the manuscript. M.M.M. was supported by fellowships of the German Academic Exchange Service, the Bavarian State government, and the Fonds der Chemischen Industrie. This work was supported in part by the NIH (GM 68550).

■ REFERENCES

(1) Benschop, H. P.; Dejong, L. P. A. *Acc. Chem. Res.* **1988**, *21*, 368.
(2) Maxwell, D.; Brecht, K.; Koplovitz, I.; Sweeney, R. *Arch. Toxicol.* **2006**, *80*, 756.
(3) Kiely, T.; Donaldson, D.; Grube, A. EPA-733-R-04-001; Washington, DC: Office of Pesticide Programs, U.S. Environmental Protection Agency, 2004.
(4) Munro, N. *Environ. Health Perspect.* **1994**, *102*, 18.
(5) Porzio, E.; Merone, L.; Mandrich, L.; Rossi, M.; Manco, G. *Biochimie* **2007**, *89*, 625.
(6) Bigley, A. N.; Raushel, F. M. *Biochim. Biophys. Acta* **2013**, *1834*, 443.
(7) Omburo, G. A.; Kuo, J. M.; Mullins, L. S.; Raushel, F. M. *J. Biol. Chem.* **1992**, *267*, 13278.
(8) Dumas, D. P.; Caldwell, S. R.; Wild, J. R.; Raushel, F. M. *J. Biol. Chem.* **1989**, *264*, 19659.
(9) Fersht, A. In *Enzyme Structure and Mechanism*, 2nd ed.; W.H. Freeman & Co.: New York, 1985; p 121.
(10) Xiang, D. F.; Kolb, P.; Fedorov, A. A.; Xu, C.; Fedorov, E. V.; Narindoshivili, T.; Williams, H. J.; Shoichet, B. K.; Almo, S. C.; Raushel, F. M. *Biochemistry* **2012**, *51*, 1762.
(11) Xiang, D. F.; Kolb, P.; Fedorov, A. A.; Meier, M. M.; Fedorov, L. V.; Nguyen, T. T.; Sterner, R.; Almo, S. C.; Shoichet, B. K.; Raushel, F. M. *Biochemistry* **2009**, *48*, 2237.
(12) Hawwa, R.; Larsen, S. D.; Ratia, K.; Mesecar, A. D. *J. Mol. Biol.* **2009**, *393*, 36.
(13) Siddavattam, D.; Khajamohiddin, S.; Manavathi, B.; Pakala, S. B.; Merrick, M. *Appl. Environ. Microbiol.* **2003**, *69*, 2533.
(14) Bigley, A. N.; Raushel, F. M. In *Handbook of Metalloproteins*; John Wiley & Sons, Ltd: New York, 2010.
(15) Elias, M.; Dupuy, J.; Merone, L.; Mandrich, L.; Porzio, E.; Moniot, S.; Rochu, D.; Lecomte, C.; Rossi, M.; Masson, P.; Manco, G.; Chabriere, E. *J. Mol. Biol.* **2008**, *379*, 1017.
(16) Bar-Even, A.; Noor, E.; Savir, Y.; Liebermeister, W.; Davidi, D.; Tawfik, D. S.; Milo, R. *Biochemistry* **2011**, *50*, 4402.
(17) Tsai, P. C.; Bigley, A.; Li, Y.; Ghanem, E.; Cadieux, C. L.; Kasten, S. A.; Reeves, T. E.; Cerasoli, D. M.; Raushel, F. M. *Biochemistry* **2010**, *49*, 7978.
(18) Steurbaut, W.; De Kimpe, N.; Schreyen, L.; Dejonckheere, W. *Bull. Chim. Belges* **1975**, *84*, 791.
(19) Ghosh, R. New Pesticidal Basic Esters of Phosphorothiolothionic Acid 1957, Patent No. GB 783281.
(20) Chapman, E.; Wong, C. H. *Bioorg. Med. Chem.* **2002**, *10*, 551.
(21) Claren, J.; Malisi, C.; Hocker, B.; Sterner, R. *Proc. Natl. Acad. Sci. U.S.A.* **2009**, *106*, 3704.
(22) Zhao, H.; Giver, L.; Shao, Z.; Affholter, J. A.; Arnold, F. H. *Nat. Biotechnol.* **1998**, *16*, 258.
(23) Ho, S. N.; Hunt, H. D.; Horton, R. M.; Pullen, J. K.; Pease, L. R. *Gene* **1989**, *77*, 51.
(24) Wang, W.; Malcolm, B. A. *Biotechniques* **1999**, *26*, 680.
(25) Davis, I. W.; Baker, D. *J. Mol. Biol.* **2009**, *385*, 381.
(26) Khare, S. D.; Kipnis, Y.; Greisen, P., Jr.; Takeuchi, R.; Ashani, Y.; Goldsmith, M.; Song, Y.; Gallaher, J. L.; Silman, I.; Leader, H.; Sussman, J. L.; Stoddard, B. L.; Tawfik, D. S.; Baker, D. *Nat. Chem. Biol.* **2012**, *8*, 294.
(27) Cleland, W. W.; Boyer, P. D., Eds.; *The Enzymes*, 3rd ed.; Academic Press: New York, 1970; Vol. 2, p 1.
(28) Nowlan, C.; Li, Y.; Hermann, J. C.; Evans, T.; Carpenter, J.; Ghanem, E.; Shoichet, B. K.; Raushel, F. M. *J. Am. Chem. Soc.* **2006**, *128*, 15892.
(29) Aharoni, A.; Griffiths, A. D.; Tawfik, D. S. *Curr. Opin. Chem. Biol.* **2005**, *9*, 210.
(30) Ben-David, M.; Elias, M.; Filippi, J. J.; Dunach, E.; Silman, I.; Sussman, J. L.; Tawfik, D. S. *J. Mol. Biol.* **2012**, *418*, 181.
(31) Benning, M. M.; Hong, S. B.; Raushel, F. M.; Holden, H. M. *J. Biol. Chem.* **2000**, *275*, 30556.
(32) Chen-Goodspeed, M.; Sogorb, M. A.; Wu, F.; Hong, S. B.; Raushel, F. M. *Biochemistry* **2001**, *40*, 1325.
(33) Afriat-Jurnou, L.; Jackson, C. J.; Tawfik, D. S. *Biochemistry* **2012**, *51*, 6047.
(34) Tokuriki, N.; Jackson, C. J.; Afriat-Jurnou, L.; Wyganowski, K. T.; Tang, R.; Tawfik, D. S. *Nat. Commun.* **2012**, *3*, 1257.
(35) Sterner, R.; Hocker, B. *Chem. Rev.* **2005**, *105*, 4038.
(36) Merone, L.; Mandrich, L.; Porzio, E.; Rossi, M.; Muller, S.; Reiter, G.; Worek, F.; Manco, G. *Bioresour. Technol.* **2010**, *101*, 9204.
(37) Gupta, R. D.; Goldsmith, M.; Ashani, Y.; Simo, Y.; Mullokandov, G.; Bar, H.; Ben-David, M.; Leader, H.; Margalit, R.; Silman, I.; Sussman, J. L.; Tawfik, D. S. *Nat. Chem. Biol.* **2011**, *7*, 120.
(38) Goldsmith, M.; Ashani, Y.; Simo, Y.; Ben-David, M.; Leader, H.; Silman, I.; Sussman, J. L.; Tawfik, D. S. *Chem. Biol.* **2012**, *19*, 456.
(39) Zhang, Y.; An, J.; Ye, W.; Yang, G.; Qian, Z.; Chen, H.; Cui, L.; Feng, Y. *Appl. Environ. Microbiol.* **2012**, *78*, 6647.
(40) Aharoni, A.; Gaidukov, L.; Kheersonsky, O.; Mc, Q. G. S.; Roodveldt, C.; Tawfik, D. S. *Nat. Genet.* **2005**, *37*, 73.
(41) Seebeck, F. P.; Hilvert, D. *J. Am. Chem. Soc.* **2003**, *125*, 10158.
(42) Khersonsky, O.; Tawfik, D. S. *Annu. Rev. Biochem.* **2010**, *79*, 471.